Steady magnetospheric convection and stream interfaces: Relationship over a solar cycle

J. Kissinger,[1] R. L. McPherron,[2] T.-S. Hsu,[2] and V. Angelopoulos[2]

Received 31 May 2010; revised 24 September 2010; accepted 19 November 2010; published 21 January 2011.

[1] Recently, an association between steady magnetospheric convection (SMC) events and solar wind stream interfaces (SI) was discovered. SMC occurrence tends to peak 0.5–1 day after a stream interface encounters the Earth, while a minimum in SMC events is seen 3–1.5 days before an SI arrives. We investigate whether this relationship holds throughout an entire solar cycle and find that during the declining phase, the relationship is consistent with previous results, while during the rising phase, no association is seen. Conditions during SMCs associated with stream interfaces are compared to unassociated SMCs, and we find differences from previous observations but consistencies with poststream interface conditions. We find that the Russell-McPherron geoeffectiveness of the solar wind stream and increased solar wind–magnetosphere coupling in the declining phase contribute to the observed association. Since SMCs usually begin with a substorm, and substorm occurrence increases both after a stream interface and during the declining phase of the solar cycle, we suggest that the increased number of substorms contributes to the higher probability of an SMC occurring during this period. The question of why coupling is greater, and why substorms occur more frequently during the declining phase, remains to be answered.

Citation: Kissinger, J., R. L. McPherron, T.-S. Hsu, and V. Angelopoulos (2011), Steady magnetospheric convection and stream interfaces: Relationship over a solar cycle, *J. Geophys. Res.*, *116*, A00I19, doi:10.1029/2010JA015763.

1. Introduction

[2] Steady magnetospheric convection (SMC) events are thought be a consequence of balanced reconnection at the dayside and nightside of the magnetosphere [*Sergeev et al.*, 1996]. These events display enhanced convection without substorm expansions, which persist for longer than a normal substorm recovery phase. The possibility of such events was first postulated by *Caan et al.* [1973], who noted that such intervals often included localized bay disturbances seen at only one or two stations. *Pytte et al.* [1978] carried out a detailed examination of one event and suggested the name "convection bay" to describe such situations. More extensive studies of this phenomenon were subsequently carried out by Sergeev and associates and are summarized by *Sergeev et al.* [1996]. In this work the name "steady magnetospheric convection" was proposed and is now more commonly used to refer to these events. However, an examination of plasma sheet convection by *Tanskanen et al.* [2005], using total magnetotail pressure to determine the convection mode, found no intervals of steady convection. Instead, they coined the term "continuous magnetospheric dissipation" (CMD) events to indicate the pressure was neither increasing nor decreasing, but relatively constant. Very recently, *DeJong et al.* [2008] proposed yet another name, "balanced reconnection intervals (BRI)" since it is now generally accepted that they are produced by balancing the rates of magnetic flux opening via dayside reconnection and flux closing via reconnection in the magnetotail. This process is sometimes referred to as the "Dungey Cycle" [*Milan et al.*, 2007] since it is the situation originally envisioned by *Dungey* [1961] to explain auroral activity.

[3] An outstanding question remains as to why the magnetosphere sometimes responds to solar wind driving with a substorm, and at other times with an SMC, even under similar conditions. *Pulkkinen et al.* [2007] used simulations to show the magnetosphere becomes less steady as solar wind speed increases. The effect of solar wind speed was confirmed with a statistical study of sawtooth events, isolated substorms, and SMCs by *Partamies et al.* [2009b]. They found that overall, solar wind conditions during SMCs are similar to substorms, but that SMCs occur during lower solar wind speed.

[4] When regions of fast solar wind impact on slow solar wind, a stream interface is created [*Gosling et al.*, 1978]. Seen at the Earth, the region of slow solar wind occurs before the interface, and a velocity increase after the interface. Therefore, one might expect to see an increase in SMC events before stream interfaces. In fact, a correlation between SMC occurrence and stream interfaces (SI) in the

[1]Department of Earth and Space Sciences, University of California, Los Angeles, California, USA.
[2]Institute of Geophysics and Planetary Physics, University of California, Los Angeles, California, USA.

0148-0227/11/2010JA015763

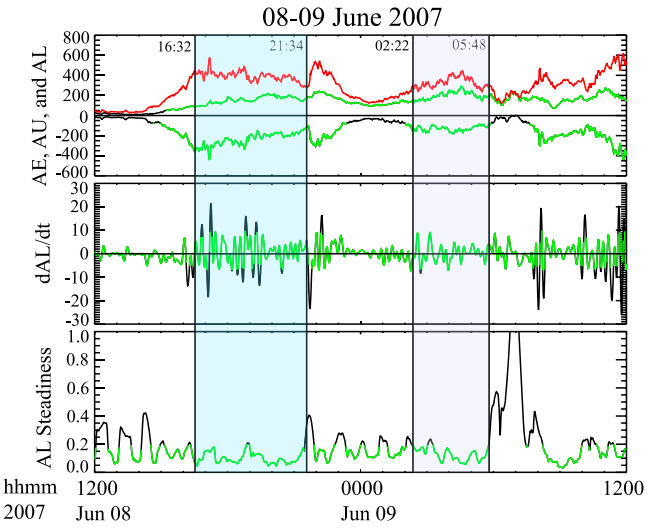

Figure 1. Two SMC intervals occurred on 8–9 June 2007. Plots of (top) *AU* and *AL*, as well as *AE* (red); (middle) d*AL*/dt, a 15 min running average representing the rate of change of *AL*; and (bottom) *AL* steadiness. Overlaid green lines show where each parameter's criterion is met. The first SMC (first blue region) begins with a substorm expansion and consists of a long recovery (5 h), while the second SMC (second blue region) does not begin with a substorm but still meets all of our criteria.

solar wind has been found for SMCs between December 2007 and April 2009 [*Kissinger et al.*, 2010]. However, the authors found that during this period, SMC occurrence peaked half a day to a day after a stream interface, not before. In addition, a minimum in SMC occurrence was seen 3–1.5 days before the stream interface. The solar wind conditions during these SMCs were different from those reported previously [*DeJong et al.*, 2009; *Partamies et al.*, 2009b; *McPherron et al.*, 2005], including faster solar wind velocity and weaker interplanetary magnetic field (IMF) B_z than expected, seeming to contradict previous results. The events of DeJong et al. and Partamies et al. were from the rising phase of the solar cycle (1997–2002 and 1998–2001, respectively) while those of McPherron et al. were from an entire solar cycle, but they did not examine the differences in SMC by solar cycle phase. Since the events of Kissinger et al. occur during the declining phase, this may explain the discrepancy between their results and the other studies. We set out to study events from Solar Cycle 23, years 1997–2008 inclusive, to determine the effect of the solar cycle on the SMC-SI relationship.

2. Event Selection

[5] In the interval 1997–2008, we identified 2951 SMC events. We adapted the auroral index criteria of *O'Brien et al.* [2002] and *Kissinger et al.* [2010] and chose events by visual inspection of the Kyoto auroral electrojet indices *AL* (auroral lower) and *AU* (auroral upper). Our requirements were as follows.

[6] 1. $AL < -75$ nT.

[7] 2. $AU > 50$ nT. This condition was ignored during the winter months due to the seasonal variation of *AU* [*McWilliams et al.*, 2008].

[8] 3. Ten nT/min > d*AL*/dt > −7.4 nT/min, where d*AL*/dt is a 15 min sliding derivative operator that represents the rate of change in the *AL* index.

[9] 4. *AL* steadiness < = 20%. Steadiness is defined as the standard deviation divided by the mean (coefficient of variance). A running average and standard deviation is found for a 30 min period, advanced by 1 min increments. A value of 0.0 indicates a completely steady interval (flat line), while higher values are less steady.

[10] 5. Event duration must be longer than 90 min in order to be longer than a typical substorm recovery period [*McPherron et al.*, 2005; *O'Brien et al.*, 2002].

[11] 6. At least 90% of data samples in a given interval satisfy all of the above criteria.

[12] All limits were selected to be larger than the magnitude of different quantities observed on a quiet day, but low enough so that we would detect small SMCs. An example of two SMC intervals on 8–9 June 2007 can be seen in Figure 1 (1631 to 2134 and 0222 to 0548). Green segments of the plotted lines show when each parameter fit the given criteria. The first event is a "typical" SMC that begins with a substorm expansion, while the second event fits all criteria but no beginning or ending substorm is seen. For both events, the *AL* index is consistently below −75 nT, and *AL* steadiness is below 20%. The first event is ended by a substorm.

[13] Stream interfaces occur when regions of faster solar wind interact with and overtake slower solar wind streams [*Gosling et al.*, 1978]. As they corotate with the Sun, they are also known as corotating interaction regions (CIRs). We identified 339 stream interfaces from 1997 to 2008 inclusive. We visually identified stream interfaces by requiring that all of the following qualitative signatures were seen in conjunction: an increase in solar wind velocity from slow (less than 500 km/s) to fast (greater than 500 km/s); an increase in density followed by a sudden drop; a bipolar variation in the azimuthal flow angle (arctan[V_y/V_x]); a peak in the magnetic field strength; increased magnitude of E_y fluctuations; and often (60% of the time) a crossing of the heliospheric current sheet as seen in the IMF spiral angle. Figure 2 shows an example of a stream interface on 19 June 1995 (not used in the study). The time of the interface was selected as the zero crossing of the azimuthal flow angle.

3. Analysis Procedure

[14] To compare our lists of SMCs and SIs, we use a technique of time delay superposed epoch analysis [*Kissinger et al.*, 2010]. For each stream interface n, we selected the SMC events that occurred after the preceding interface ($n-1$) and before the subsequent interface ($n+1$). We calculated the delay between the SMCs and the nth stream interface, and accumulated the delays for each SI. A histogram of the time delays was generated, separated into 0.5 day (12 h) bins, and spanning −20 days (before a stream interface) to +20 days (after a stream interface). To construct a probability density

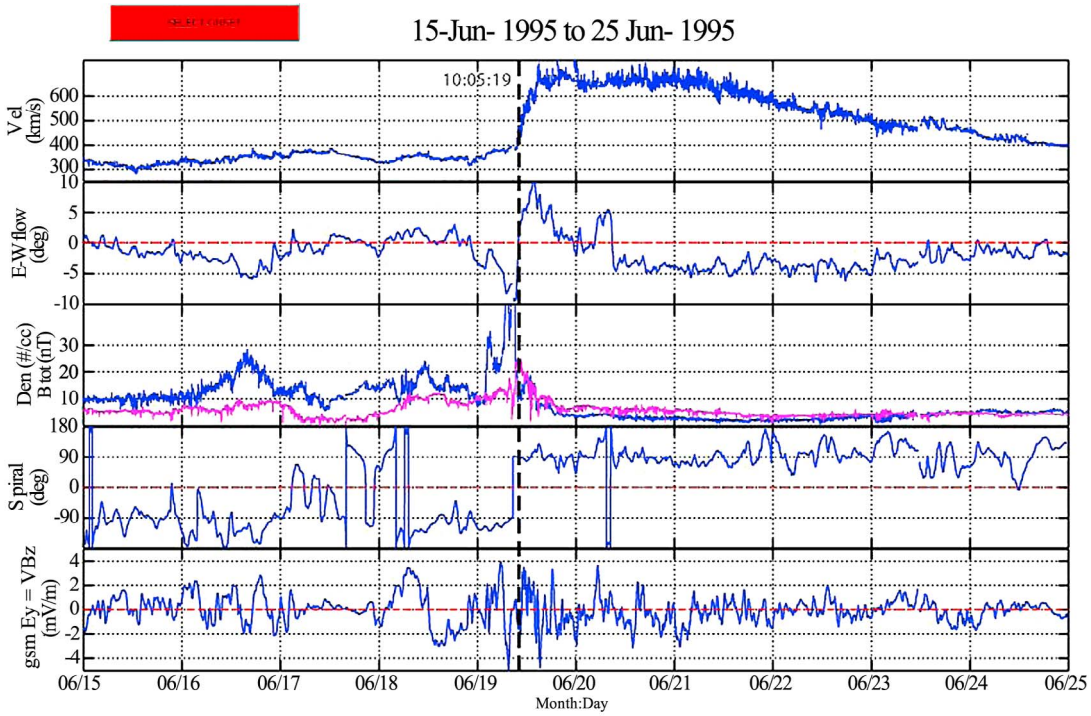

Figure 2. Example of a stream interface. Solar wind OMNI data is plotted during June 1995: total velocity, east-west flow angle, IMF magnitude (pink) and density (blue), spiral angle, and GSM E_y. The time of the interface (1005:19) was selected at the zero crossing of the flow angle. Velocity increases sharply from ~380 km/s to over 600 km/s. An increase is seen in density before the interface, followed by a sudden drop, and B_{total} increases after the interface. The spiral angle shows that there is a crossing of the heliospheric current sheet.

histogram, we divided the time delay histogram by the total number of delays times the bin width:

$$\text{PDH} = \text{Histogram}/(\text{number of delays*bin width})$$

Plotting the probability density histogram results in a superposed epoch analysis of SMC occurrence with respect to the time of stream interfaces (t = 0, see Figure 3).

[15] This procedure introduces artifacts into the analysis. First, delays are found only for SMCs that occur between the preceding and following SIs; therefore, any SMCs outside this range are ignored. If our SIs were evenly spaced by 7 days, for example, this means it would be impossible to get a delay of more than ±7 days. Although stream interfaces have a typical recurrence rate (7 days over the entire solar cycle), they are irregularly spaced, and thus SMC events are seen past this average SI recurrence time. The delays in the histogram fall off rapidly after 7 days, and because there are few events there we ignore anything near the outskirts of the graph.

[16] Second, an SMC event with a positive delay for the *n*th interface (event occurring after the stream interface) will in turn have a negative delay for the *n*th+1 interface (event before the stream interface). This effectively doubles the number of events—an SMC will appear twice on either side of the t = 0 line. Combining this with the above "average SI recurrence time" can result in a secondary peak at −7 days. This is an effect of the analysis and does not appear when the relationship is examined using other methods.

4. Dependence of the SMC-SI Relationship on Solar Cycle

[17] Plots of SMC occurrence using time delay superposed epoch analysis were examined for each year from 1997 to 2008. A comparison of these yearly graphs revealed that SMC occurrence with respect to SIs showed two types of behavior—correlated and uncorrelated—and that these were organized by solar cycle phase. Figure 3 displays the probability density of an SMC occurring at various times with respect to a stream interface (epoch time = 0, thick vertical dashed line) in 12 h bins, with the two traces corresponding to different phases of the solar cycle. The rising phase (1997–2003, blue line), shows no correlation between SMCs and stream interfaces, while the declining phase (2004–2008, red line) shows a significant organization of SMC with respect to stream interfaces. In this case, SMC occurrence peaks sharply 0.5–1 day after a stream interface, and there is a minimum in SMC occurrence −2.5 to −1 days before the interface. This is similar to the result found by *Kissinger et al.* [2010] for 2008 data. The gray bar graph is a histogram of separation between successive SI. The most probable separation between SI is 7 days, shown as a thin dashed line before and after epoch zero. The small peak in

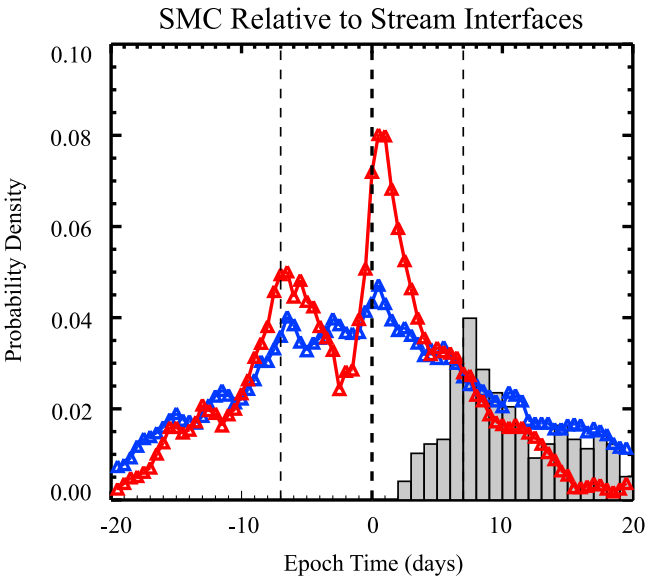

Figure 3. SMC intervals are compared with stream interfaces using time delay analysis. Epoch t = 0 marks a stream interface (thick vertical dashed black line). The probability density of occurrence of SMCs in the days before and after an interface is plotted in 12 h intervals. The rising phase of the solar cycle, years 1997–2003, is plotted with the blue line, and the declining phase, 2004–2008, is the red line. The separation of successive stream interfaces in days is shown as a gray histogram, and the most probable separation (7 days) is plotted before and after t = 0 as a thin vertical dashed line.

the rising phase was found to be not significant when examined with other methods. Again, the secondary declining phase peak at −7 days is an artifact of the analysis.

[18] Why are SMCs correlated with stream interfaces during the declining phase of the solar cycle, but not during the rising phase? One possibility is that the stream interfaces themselves are different during different parts of the solar cycle. Figure 4 again shows the probability density of SMC occurrence with respect to stream interfaces, now separated by phase (rising phase on the left, declining phase on the right) and by geoeffectiveness of the streams according to the Russell-McPherron effect [*Russell and McPherron*, 1973]. Effectiveness of the solar wind to reconnect with the Earth's magnetosphere depends on the changing orientation of the solar magnetospheric coordinate system relative to the solar equatorial system. It can be determined by the magnetic spiral angle according to the rule "Spring To, Fall Away" [*Russell and McPherron*, 1973]. During the spring equinox, the solar wind is geomagnetically effective when the magnetic field points toward the Earth, and ineffective when it points away from the Earth; during the fall it is the opposite. The solar wind can be ineffective or effective both before and after the interface, thus there are four categories: effective before, effective after (EE, first row, black lines); ineffective before, effective after (IE, second row, red lines); effective before, ineffective after (EI, third row, green lines); and ineffective before and ineffective after (II, fourth row, blue lines). The type of interface and the number associated are displayed on each plot.

[19] In the rising phase of cycle 23, EE interfaces were the most likely to occur (although all types have around the same occurrence rate except for II, which occurs less often). Relative to IE interfaces, there is a jump in SMC occurrence just before the interface, while EE, EI, and II and II show no correlation with SMCs. In the declining phase, the number of EE interfaces dropped by a factor of two, and IE is the most frequently occurring type of stream interface. Note that seven years of data goes into the rising phase plots, while only five years of data appears in the declining phase, meaning that the number of SIs per year increases over the solar cycle. Both EE and IE show a peak in SMC occurrence at/after the interface, especially IE. This SMC peak after EE interfaces is not seen in the rising phase. SMC occurrence near EI interfaces is flat, although there is a tendency for increased SMC occurrence 5–7 days before the interface. Finally, although occurrence at II interfaces is relatively flat, it shows a small peak in SMC right after the interface.

[20] During the declining phase, there are more IE than EE interfaces, while during the rising phase, EE is most prominent. It might be that the interface type that occurs most often determines what behavior is seen overall in Figure 3. Why is there a difference in stream interface behavior between the two phases? The occurrence of EE changes drastically, and in the declining phase, two interface types show a definite peak after the interface (EE, IE), while only one does in the rising phase (IE). Even the SMC peaks for IE interfaces change significantly. This suggests there is still an unknown difference between phases, especially for EE and IE interfaces.

[21] Figure 5 shows superposed epoch analysis of solar wind and ground station parameters, where stream interfaces occur at t = 0 days. The interfaces are separated by effectiveness type, as evidenced by the first panel, spiral angle (Psi). This angle results from a coordinate system rotated +45° about Z_{GSE}, so that angles near −90° are "toward" (effective in Spring) and angles near +90° are "away" (ineffective in Spring). The spiral angle has been flipped for data in the fall in order to agree with this convention. Here it is easy to see that EE interfaces are effective before and after the interface; IE interfaces are ineffective before and switch to being effective just before the interface, and so on. The remaining panels display solar wind dynamic pressure ($p_{dyn} = 1.67 \times 10^{-6} n_p v^2$), solar wind GSM E_y, *AE* index, and *Sym-H* index. There is a higher dynamic pressure peak associated with the two interface types that include an IMF sector crossing, IE and EI, which occurs during ~60% of stream interfaces. This results from the crossing of the heliospheric current sheet (HCS), which is a region of enhanced density separating the two different regions of magnetic polarity [*Bavassano et al.*, 1997]. Note that geoeffective high-speed streams (EE, black and IE, red) result in higher geomagnetic activity after the interface (*AE* and *Sym-H*) than ineffective. The largest increase in activity is caused by IE, and the smallest by EI. This is due to the fact that the two types which are effective after the interface, IE (73 interfaces) and EE (50 interfaces), show positive E_y afterward, while streams which are ineffective after (47 II and 70 EI) have negative E_y GSM. In fact, effective after interfaces (EE, IE) result in stronger E_y signatures after the stream interface

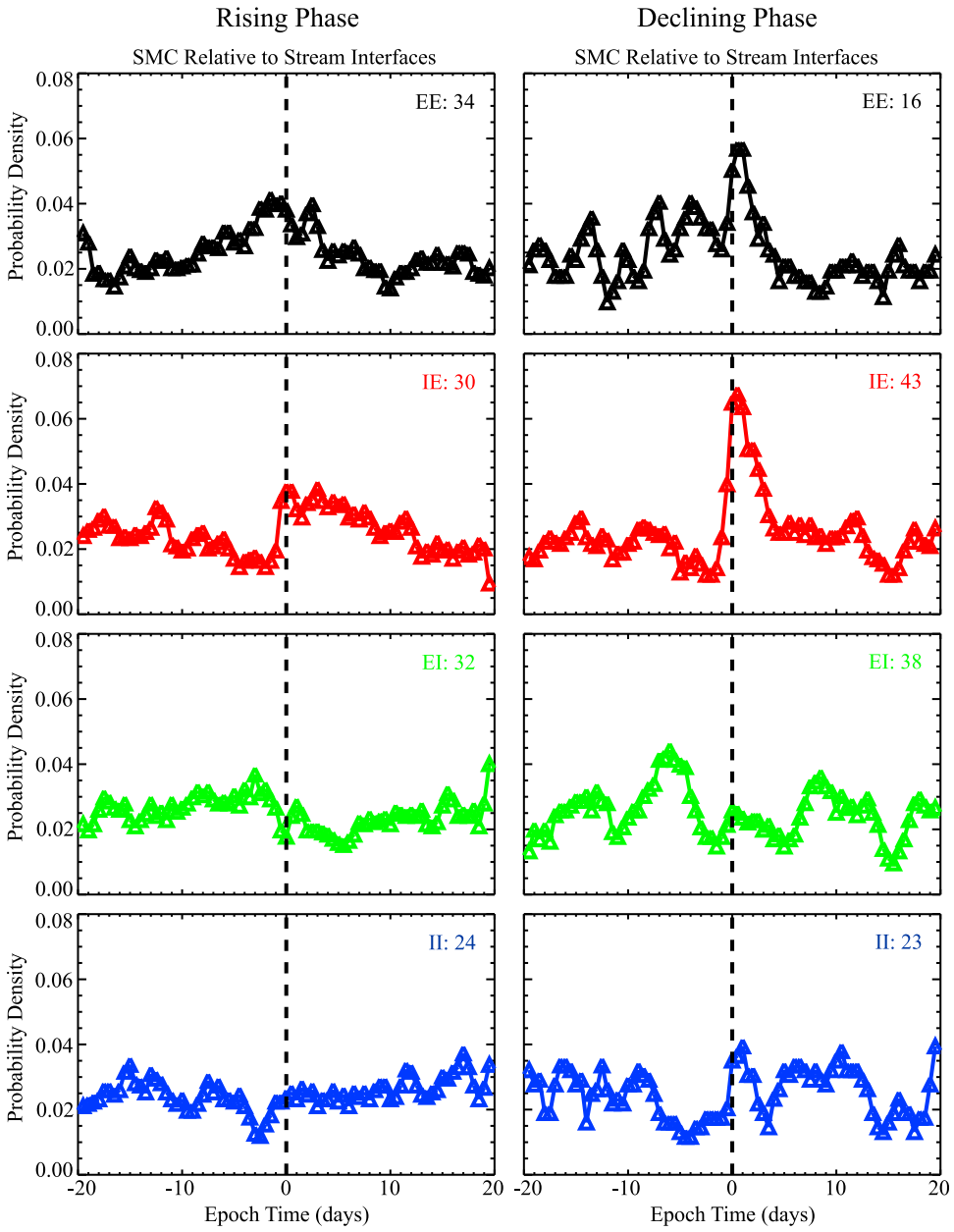

Figure 4. SMC probability density before and after stream interfaces is plotted in 12 h bins by (left) rising phase and (right) declining phase and by stream effectiveness: EE (black, first row), IE (red, second row), EI (green, third row), and II (blue, fourth row). The number of interfaces for each case is displayed on its respective plot.

than effective before interfaces (EE, EI) show before the event, owing to the increase in velocity. This is consistent with the Russell-McPherron statement that geomagnetic activity is organized by effectiveness of the IMF. EE and IE interfaces correlate with SMC activity because their effective solar wind orientation after the interface results in more negative B_z/more positive E_y, resulting in reconnection, and a higher probability of SMCs.

[22] The increase in reconnection during a geoeffective high-speed stream affects other types of activity as well. Using a list of over 20000 substorm onsets [*Hsu et al.*, 2009], we compared the number of substorms that occur before and after a stream interface. This is shown in Figure 6 as substorm number versus time. The number of substorms that occur within 2 days before each interface is plotted as a thin green line, and those occurring within 2 days after an interface in a thin blue line. Smoothing of these lines was accomplished by creating a NaN (not a number) time series with 1 day resolution. For each SI onset, the substorm number occurrence before and after was filled into the time series, and then a running average using a ±40 days time window was calculated. The running averages are superimposed on the raw time series as a thick red line (before SI) and thick blue line (after SI). There are always

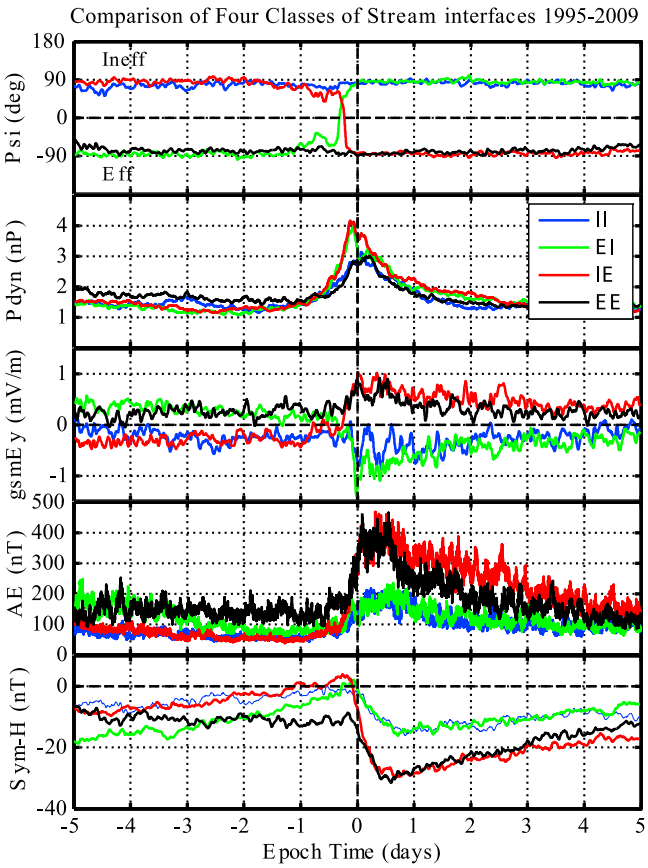

Figure 5. Superposed epoch analysis with respect to stream interfaces of IMF spiral angle, dynamic pressure, GSM E_y, *AE* index, and *Sym-H*. Interfaces are separated by effectiveness: II (blue), EI (green), IE (red), and EE (black).

more substorms after a stream interface than before it. The upward trend suggests that there are more substorms in the declining phase of the solar cycle than in the rising phase. There seems to be a periodicity in the number of substorms on the order of 1–1.5 years which should be explored in the future.

5. Solar Wind–Magnetosphere Coupling

[23] The solar wind causes geomagnetic activity in the form of a half-wave rectifier [*Murayama et al.*, 1980]. When the IMF points southward, it couples to the Earth's magnetic field via reconnection. Solar wind–magnetosphere coupling is more efficient during SMC events than other modes of response [*Partamies et al.*, 2009a]. The magnetosphere can be thought of as a driven system, with the solar wind rectified E_y as the input ($E_y > 0$, corresponding to $B_z < 0$ since $E_y \sim V_x B_z$; also called E_s), and the convection in the magnetosphere, approximated by *AL* index, as the output. If we assume that the filter is causal, the impulse response of the magnetosphere can be represented as

$$O(t) = (I^{*}g)(t) \stackrel{\text{def}}{=} \int_{-\infty}^{\infty} I(\tau)g(t-\tau)d\tau$$

where O is the output of the system, I is the input of the system, g is the impulse response function integrated over time, and τ is the variable of integration in the convolution equation. To attain an estimate of the coupling between E_y and *AL*, we assumed that the input I = E_y(t) and the output O = *AL*(t) during an event were constant. This allows us to take I(t) outside the integral. The integral then becomes the area under the impulse response function $g(\tau)$ which we call the coupling constant. This constant is the ratio of average *AL* to average E_y. To examine the coupling efficiency of our data set, we selected SMC events that were at least 2 h long and required that E_y was positive 95% of the time. We averaged all data after the first hour of the SMC to partially remove any transient effects. The smoothed probability density function (calculated in the same manner as Figure 3) of the coupling constant = AL_{avg}/E_{savg} is shown in Figure 7. The rising phase is in blue, and the declining phase is in red. The most probable value for each phase is plotted as dashed lines with the value annotated next to the line.

[24] The measure of the coupling is greater during the declining phase than during the rising phase. This means that the same E_y value (input) resulted in a larger *AL* index value (output) during the latter part of the solar cycle. This concurs with a similar result found by *McPherron et al.* [2009] using a more robust analysis of time-dependent linear prediction filters. They suggest various explanations, including low quality of *AL* index during the rising phase or the increase of CMEs during the rising phase and at maximum with different properties than CIRs. In fact, *Turner et al.* [2009] found that CIR-driven storms are more efficient than those driven by CMEs. Since CME occurrence decreases during the declining phase [*Webb and Howard*, 1994], we may be seeing the effect of CIR efficiency becoming more prominent. While this may explain the results for overall coupling efficiency, we found no significant correlation between SMCs and CMEs, so it is difficult to determine how the lack of CMEs affects the coupling efficiency of SMCs in the declining phase. A third option for increased coupling offered by McPherron et al. is that some of the *AL* variance is due to viscous interaction, dynamic pressure, or electron precipitation. Energetic electrons in the magnetosphere [*Vassiliadis et al.*, 2002, paragraph 42] and solar wind dynamic pressure [*Fairfield and Jones*, 1996, Figure 6] do peak during the declining and minimum phases of the solar cycle. This increase in declining phase coupling may also explain why there are more substorms during the declining phase (Figure 6). The particular mechanisms that cause increased coupling in the declining phase should be examined in future studies.

6. SMCs Associated and Unassociated With Stream Interfaces

[25] SMCs selected by *Kissinger et al.* [2010] were found to occur during very different solar wind conditions than in previous studies [*O'Brien et al.*, 2002; *DeJong et al.*, 2009]. To examine solar wind and geomagnetic conditions for our list, we divided our SMCs into associated (occurring between 0 and 2 days after a stream interface) and unassociated events (all other days). The probability of associated events changed significantly between solar cycle phases:

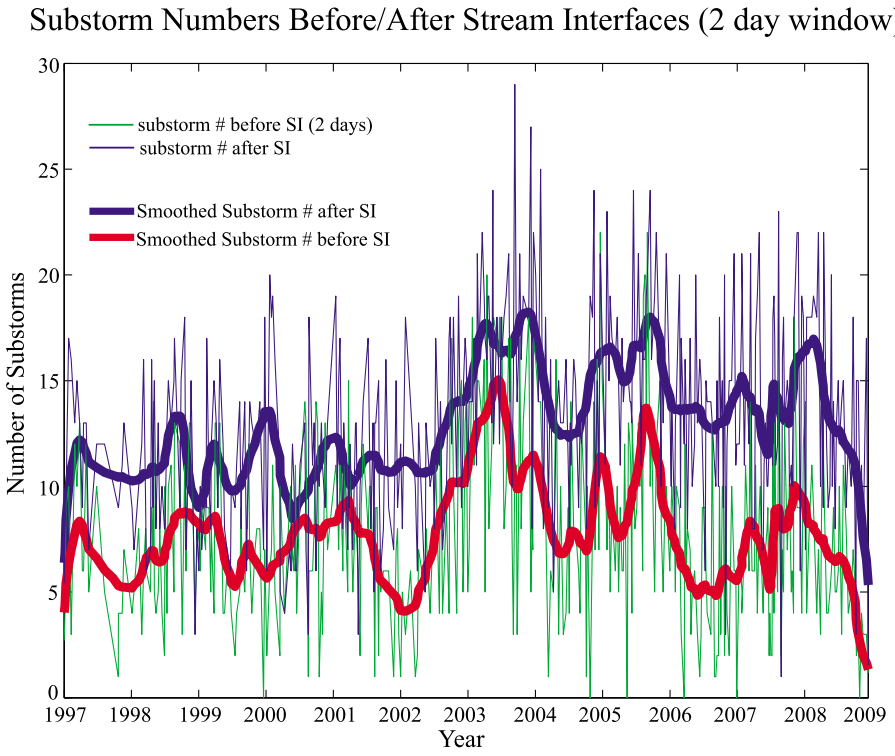

Figure 6. Number of substorms versus time over a solar cycle. Substorms that occur 2 days before a stream interface are plotted in green; substorms that occur 2 days after are plotted in blue (thin line). The smoothed number of substorms before (red) and after (blue) are overlaid in thick lines.

288 out of 1848 SMCs were associated with stream interfaces during the rising phase (~15.6%), but 336 out of 1103 SMCs were associated during the declining phase (~30.5%), a twofold increase. This reiterates the result that SMCs are significantly associated with stream interfaces in the declining phase.

[26] We used 1 min WIND and Kyoto data to compare the two types of events. For each parameter, a cumulative probability distribution function (cdf) was calculated for associated SMCs, unassociated SMCs, and background (all other data). This was further split into solar cycle rising phase and declining phase, as in sections 4 and 5. In order to determine whether two different distributions are significantly different, we utilized the Kolmogorov-Smirnov test (KS test) [*Press et al.*, 1986]. The KS statistic is the maximum value of the absolute difference between two cdfs $S_{N1}(x)$ and $S_{N2}(x)$:

$$D = \max_{-\infty<x<\infty} |S_{N1}(x) - S_{N2}(x)|$$

To find the significance of D, one uses the following sum:

$$Q_{KS}(\lambda) = 2\sum_{j=1}^{\infty}(-)^{j-1}e^{-2j^2\lambda^2}$$

This is a monotonic function with limiting values. If $\lambda = 0$, then $Q_{KS} = 1$; if $\lambda = \infty$, $Q_{KS} = 0$. The significance level of D is given by

$$Probability(D > observed) = Q_{KS}\left(\sqrt{\frac{N_1N_2}{N_1+N_2}}D\right)$$

where N_1 is the number of data points in the first distribution, and N_2 is the number in the second. Small probability values show that the cdfs are significantly different. This becomes asymptotically accurate as the two Ns grow large. Since we are dealing with 1 min data over a period of several years, we have a very large number of samples that make up each cdf. Using the KS test to compare our cdfs, we never resulted in a

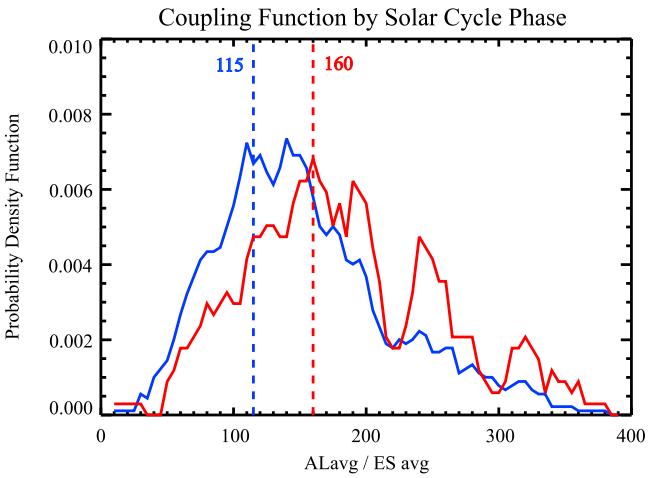

Figure 7. Probability density function of coupling constant (AL_{avg}/ES_{avg}), separated by phase (rising, blue line; declining, red line). The most probable value for each phase is displayed as a number and vertical dashed line.

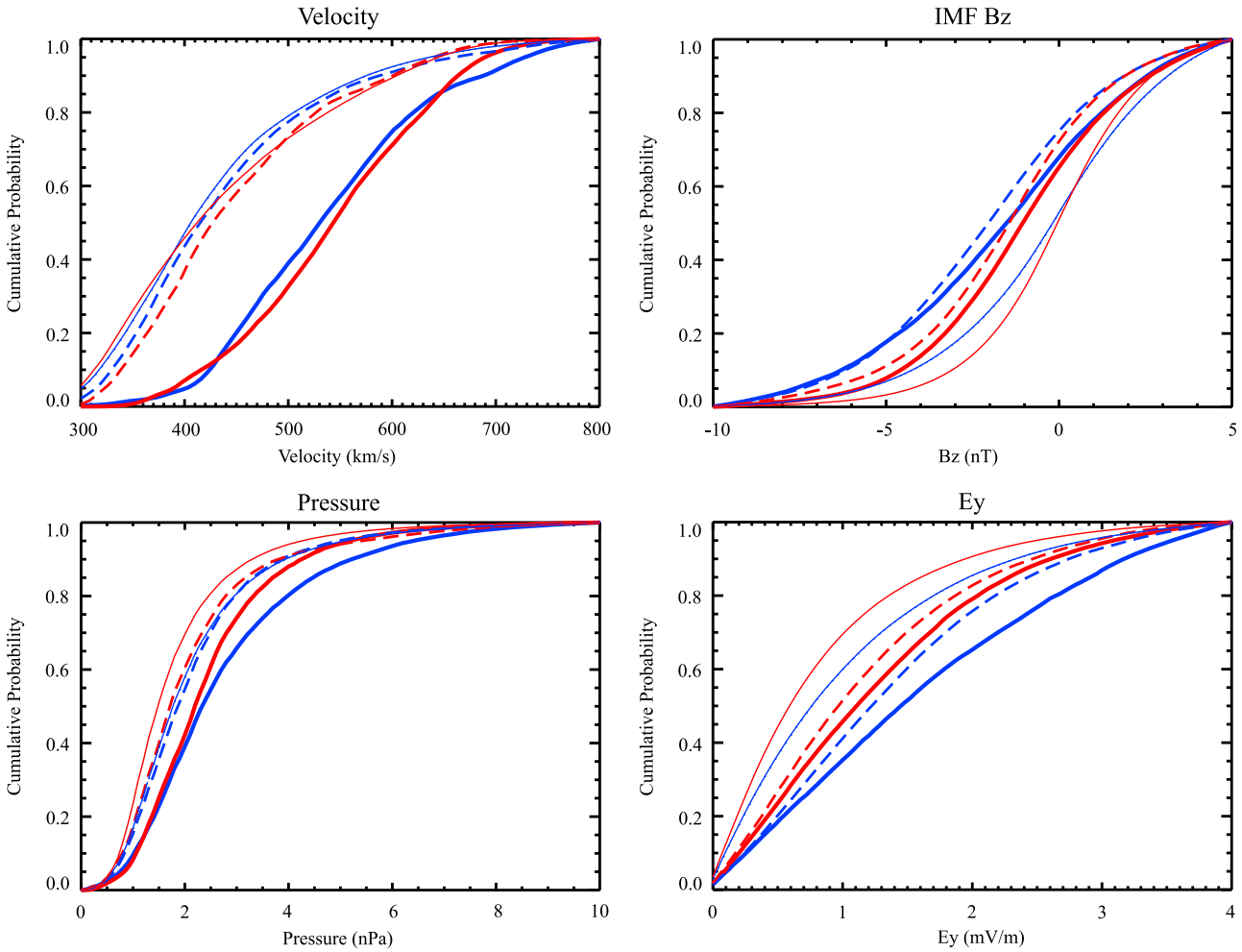

Figure 8. Cumulative probability distributions of solar wind total velocity, dynamic pressure, IMF B_z, and rectified E_y. Blue lines correspond to rising phase (1997–2003), and red lines correspond to declining phase (2004–2008). Solid thick lines represent data during associated SMCs (those that occur within 2 days after a stream interface), dashed lines represent data during unassociated SMCs, and solid thin lines represent all other data (background).

probability larger than 1×10^{-7}—in fact, for many comparisons the exponential grew so large that the probability was evaluated to 0. Due to our large sample numbers, even small differences between two cdfs are significant.

[27] Figure 8 shows the cumulative probability distribution functions of solar wind total velocity (V_t), dynamic pressure (P_{dyn}), IMF $B_{z,GSM}$, and rectified E_y (only positive values to correspond to negative B_z). The rising phase is plotted in blue, and the declining phase is in red. Solid thick lines represent associated SMCs, dashed lines represent unassociated SMCs, and solid thin lines plot all other data, which can be considered the solar wind background. Figure 9 plots the cumulative probability distribution functions in the same convention and for the same parameters as in Figure 8, but for their steadiness (standard deviation/mean). A larger steadiness parameter means that the data is less steady, and a smaller parameter is steadier. Data with steadiness parameter = 0 would be a straight line. Associated SMCs occur during much faster and less steady solar wind than unassociated SMCs. This is due to the definition of a stream interface as a jump from slower to faster velocity. In addition, associated SMC events, compared to unassociated, occur during weaker, less steady B_z; stronger, less steady E_y; and slightly higher pressure and lower density (not shown). The differences match conditions expected after a stream interface, but represent a departure from typical SMC conditions [*McPherron et al.*, 2005; *DeJong et al.*, 2009]. When we combine both types of SMCs, the solar wind parameters are similar to these prior studies, so associated SMC events may be averaged out in other research.

[28] Conditions during unassociated SMCs occur during slow and steady solar wind velocity, similar to background levels, and for moderately negative, steadier B_z and positive, steadier E_y compared to the background. For the most part, this agrees with previous studies [*O'Brien et al.*, 2002; *McPherron et al.*, 2005; *DeJong et al.*, 2009]; however, both DeJong et al. and O'Brien et al. found that solar wind velocity during SMCs is slower compared to the background, while for our unassociated SMCs the velocity is in

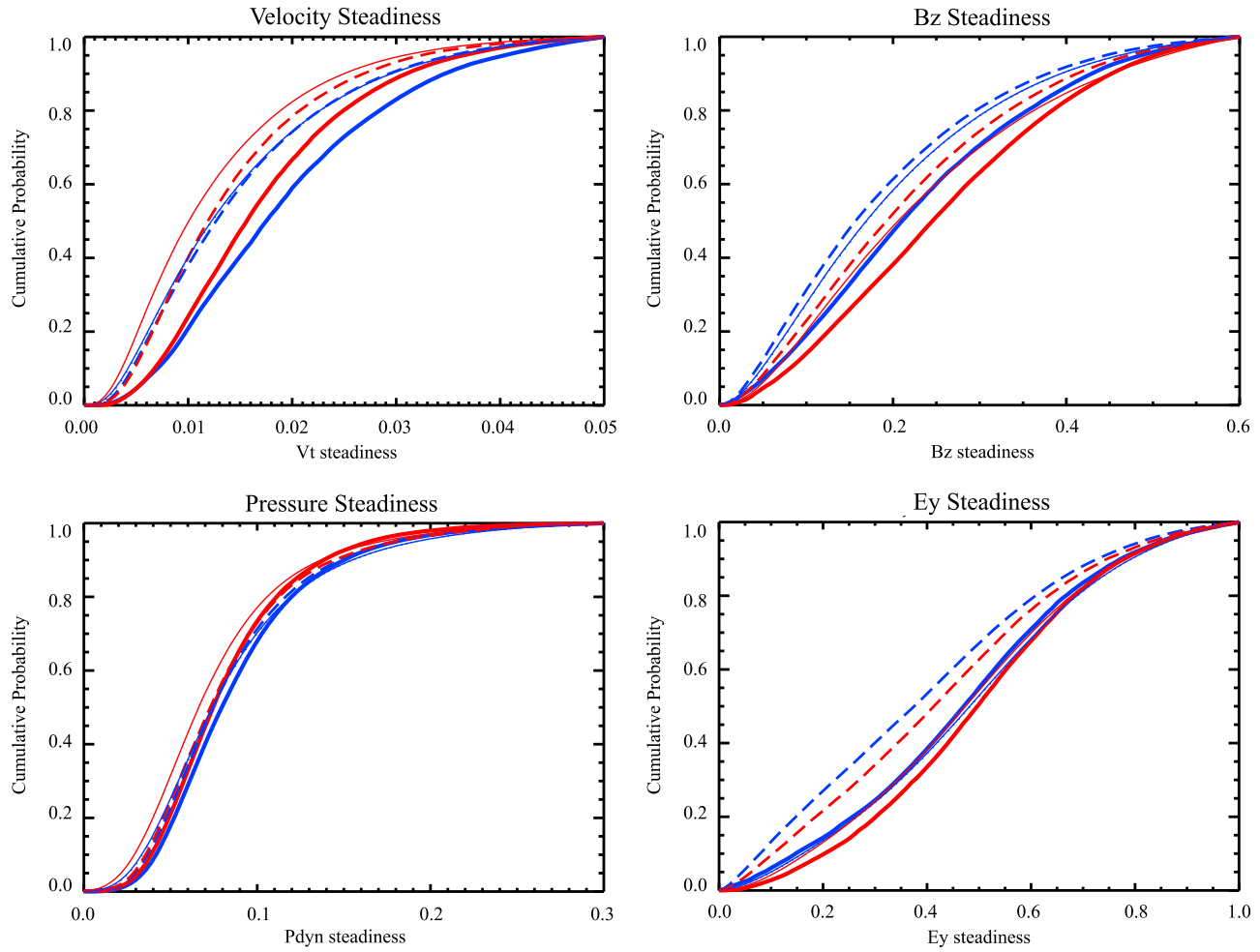

Figure 9. Cumulative probability distributions of solar wind total velocity steadiness, dynamic pressure steadiness, IMF B_z steadiness, and rectified E_y steadiness, following the same convention as Figure 8.

fact comparable to or slightly faster than the background. What could cause this difference in velocity behavior, especially given that DeJong et al. used BRIs during 1997–2002, which nearly overlaps our rising phase period (1997–2003)? When we compare velocity cdfs by year, the only year in which unassociated SMC velocity is faster than the background is in 2003. Solar wind velocity during 2003 was unusually high [*Gibson et al.*, 2009, Figure 3a], and this abnormal year increases the overall average of the rising phase unassociated SMC velocity.

[29] *DeJong et al.* [2009] found that occurrence of different modes of magnetospheric response depended most on the magnitude of the solar wind velocity (<450 km/s for SMCs) and the magnitude (~4 nT) and steadiness (steady) of the IMF B_z. Our unassociated SMCs agree with these figures, while associated SMCs occur during faster solar wind (due to their appearance after stream interfaces) and have less steady IMF B_z than the background. E_y steadiness during associated SMCs is comparable to the background—it is neither less steady nor more steady—while for other parameters associated SMCs are less steady than the background. This suggests that it is steady E_y that results in SMCs. Overall, SMC solar wind conditions during the declining phase of the solar cycle, compared to the rising phase, have slightly faster, steadier V_t; weaker, less steady B_z; weaker, less steady E_y; and slightly lower pressure and density.

[30] The cumulative probability distribution functions for geomagnetic *AL* and *AU* are plotted in Figure 10, along with their steadiness. These plots also follow the conventions of Figure 8. Both types of SMCs, by nature of their selection criteria, have enhanced, steadier *AL* and *AU* indices compared to all non-SMC data. Associated SMCs have stronger *AL* and *AU* values than unassociated. The steadiness of *AL* is the same for either type of SMC, but associated SMCs have less steady *AU* than unassociated. Both auroral electrojet indices tend to be weaker and less steady in the declining phase.

7. Conclusions

[31] We have found a correlation between steady magnetospheric convection events and stream interfaces in the solar wind. SMC occurrence peaks 0.5–1 day after a stream interface. A minimum in SMC events is seen 3–1.5 days before the interface. This correlation is present in the declining phase of solar cycle 23, but during the rising phase

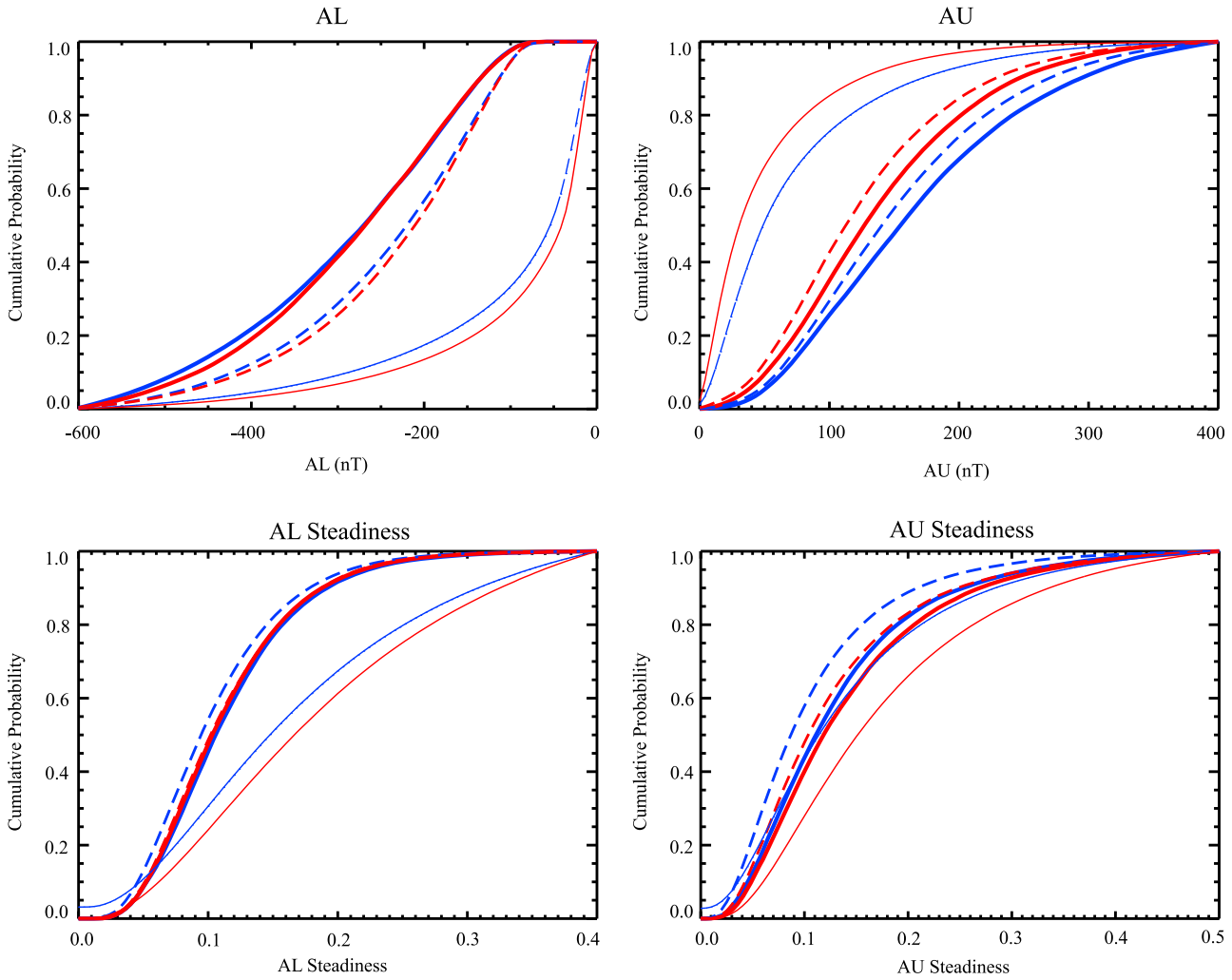

Figure 10. Cumulative probability distributions of *AL*, *AL* steadiness, *AU*, and *AU* steadiness, following the same convention as Figure 8.

no change in SMC occurrence is seen with respect to stream interfaces.

[32] There are several factors that contribute to the different correlation between phases. First, the IMF geoeffectiveness of the stream influences SMC occurrence. Streams that are effective after the interface (EE and IE) tend to have higher positive E_y values that will result in reconnection, and correspondingly larger geomagnetic activity. In the declining phase, two types of interfaces show a correlation with SMC occurrence, EE and IE. In the rising phase, only IE exhibit a correlation. The most commonly occurring type of interface also changes by phase, and this appears to determine which association is seen in the aggregate. In the rising phase, EE occurs most often, while in the declining phase, the most common type is IE. The reason for this change in stream interface geoeffective type by phase is a question to be examined in future research. A second factor for SMC-SI correlation is the occurrence of substorms. More substorms occur after a stream interface than before, and substorm occurrence increases during the declining phase [*Hsu et al.*, 2009]. Most SMCs begin with a substorm, and therefore there is a greater chance of SMCs occurring after a stream interface in the declining phase. Third, solar wind–magnetosphere coupling is stronger during the declining phase. The reason for this is unknown and will be explored later.

[33] These factors result in SMCs that are associated with stream interfaces. This is the first time such a subpopulation of SMCs has been identified. The subset occurs during different solar wind conditions than previous studies reported [*O'Brien et al.*, 2002; *DeJong et al.*, 2009], but we suggest that they have been averaged out in other research. In particular the solar wind velocity is very high, far beyond the ranges expected for SMC, and all parameters are less steady. This is due to the SMCs' following a stream interface, but is unexpected since *McPherron et al.* [2005] show that slow, steady solar wind results in SMCs. The declining phase SMC-SI relationship and its causes above must be further studied to determine why these different solar wind conditions result in SMCs.

[34] **Acknowledgments.** We thank the World Data Center for Geomagnetism, Kyoto, for the use of the provisional *AL* and *AU* data and

Joseph King and Natasha Papitashvili for providing OMNI data through the NASA NSSDC. This paper is based upon work supported by the National Science Foundation under agreement ATM-0720422, by NASA NNX07AF60G, and by the THEMIS program, supported by NASA contract NAS5–02099.

[35] Philippa Browning thanks the reviewers for their assistance in evaluating this paper.

References

Bavassano, B., R. Woo, and R. Bruno (1997), Heliospheric plasma sheet and coronal streamers, *Geophys. Res. Lett.*, *24*(13), 1655–1658, doi:10.1029/97GL01630.

Caan, M. N., R. L. McPherron, and C. T. Russell (1973), Solar wind and substorm-related changes in the lobes of the geomagnetic tail, *J. Geophys. Res.*, *78*(34), 8087–8096, doi:10.1029/JA078i034p08087.

DeJong, A. D., A. J. Ridley, and C. R. Clauer (2008), Balanced reconnection intervals: Four case studies, *Ann. Geophys.*, *26*, 3897–3912, doi:10.5194/angeo-26-3897-2008.

DeJong, A. D., A. J. Ridley, X. Cai, and C. R. Clauer (2009), A statistical study of BRIs (SMCs), isolated substorms, and individual sawtooth injections, *J. Geophys. Res.*, *114*, A08215, doi:10.1029/2008JA013870.

Dungey, J. W. (1961), Interplanetary magnetic field and the auroral zones, *Phys. Rev. Lett.*, *6*(2), 47–48, doi:10.1103/PhysRevLett.6.47.

Fairfield, D. H., and J. Jones (1996), Variability of the tail lobe field strength, *J. Geophys. Res.*, *101*(A4), 7785–7791, doi:10.1029/95JA03713.

Gibson, S. E., J. U. Kozyra, G. De Toma, B. A. Emery, T. Onsager, and B. J. Thompson (2009), If the Sun is so quiet, why is the Earth ringing? A comparison of two solar minimum intervals, *J. Geophys. Res.*, *114*, A09105, doi:10.1029/2009JA014342.

Gosling, J., J. Asbridge, S. Bame, and W. Feldman (1978), Solar wind stream interfaces, *J. Geophys. Res.*, *83*(A4), 1401–1412, doi:10.1029/JA083iA04p01401.

Hsu, T.-S., R. L. McPherron, J. Kissinger, M. G. Kivelson, V. Angelopoulos, H. Zhang, and Y. Ge (2009), An investigation of the solar cycle effect on substorms, *Eos Trans. AGU*, *90*(52), Fall Meet. Suppl., Abstract SM13B–1599.

Kissinger, J., R. L. McPherron, V. Angelopoulos, T.-S. Hsu, and J. P. McFadden (2010), An investigation of the association between steady magnetospheric convection and CIR stream interfaces, *Geophys. Res. Lett.*, *37*, L04105, doi:10.1029/2009GL041541.

McPherron, R. L., T. P. O'Brien, and S. M. Thompson (2005), Solar wind drivers for steady magnetospheric convection, in *Multiscale Coupling of the Sun-Earth Processes*, edited by A. T. Y. Liu, Y. Kamide, and G. Consolini, pp. 113–124, Elsevier, Amsterdam, doi:10.1016/B978-044451881-1/50009-5.

McPherron, R. L., L. Kepko, T. I. Pulkkinen, T.-S. Hsu, J. W. Weygand, and L. F. Bargatze (2009), Changes in the response of the AL index with solar cycle and epoch within a corotating interaction region, *Ann. Geophys.*, *27*, 3165–3178, doi:10.5194/angeo-27-3165-2009.

McWilliams, K. A., J. B. Pfeifer, and R. L. McPherron (2008), Steady magnetospheric convection selection criteria: Implications of global SuperDARN convection measurements, *Geophys. Res. Lett.*, *35*, L09102, doi:10.1029/2008GL033671.

Milan, S. E., G. Provan, and B. Hubert (2007), Magnetic flux transport in the Dungey cycle: A survey of dayside and nightside reconnection rates, *J. Geophys. Res.*, *112*, A01209, doi:10.1029/2006JA011642.

Murayama, T., T. Aoki, H. Nakai, and K. Hakamada (1980), Empirical formula to relate the auroral electrojet intensity with interplanetary parameters, *Planet. Space Sci.*, *28*(8), doi:10:1016/0032-0633(80)90078-1.

O'Brien, T. P., S. M. Thompson, and R. L. McPherron (2002), Steady magnetospheric convection: Statistical signatures in the solar wind and *AE*, *Geophys. Res. Lett.*, *29*(7), 1130, doi:10.1029/2001GL014641.

Partamies, N., T. I. Pulkkinen, R. L. McPherron, K. McWilliams, C. R. Bryant, E. Tanskanen, H. J. Singer, G. D. Reeves, and M. F. Thomsen (2009a), Statistical survey on sawtooth events, SMCs and isolated substorms, *Adv. Space Res.*, *44*, 376–384, doi:10.1016/j.asr.2009.03.013.

Partamies, N., T. I. Pulkkinen, R. L. McPherron, K. McWilliams, C. R. Bryant, E. Tanskanen, H. J. Singer, G. D. Reeves, and M. F. Thomsen (2009b), Different magnetospheric modes: Solar wind driving and coupling efficiency, *Ann. Geophys.*, *27*, 4281–4291, doi:10.5194/angeo-27-4281-2009.

Press, W. H., B. P. Flannery, S. A. Teukolsky, and W. T. Vetterling (1986), *Numerical Recipes*, Cambridge Univ. Press, New York.

Pulkkinen, T. I., C. C. Goodrich, and J. G. Lyon (2007), Solar wind electric field driving of magnetospheric activity: Is it velocity or magnetic field?, *Geophys. Res. Lett.*, *34*, L21101, doi:10.1029/2007GL031011.

Pytte, T., R. L. McPherron, E. W. Hones Jr., and H. I. West Jr. (1978), Multiple-satellite studies of magnetospheric substorms: Distinction between polar magnetic substorms and convection-driven negative bays, *J. Geophys. Res.*, *83*(A2), 663–679, doi:10.1029/JA083iA02p00663.

Russell, C. T., and R. L. McPherron (1973), Semiannual variation of geomagnetic activity, *J. Geophys. Res.*, *78*(1), 92–108, doi:10.1029/JA078i001p00092.

Sergeev, V. A., R. J. Pellinen, and T. I. Pulkkinen (1996), Steady magnetospheric convection: A review of recent results, *Space Sci. Rev.*, *75*, 551–604, doi:10.1007/BF00833344.

Tanskanen, E. I., J. A. Slavin, D. H. Fairfield, D. G. Sibeck, J. Gjerloev, T. Mukai, A. Ieda, and T. Nagai (2005), Magnetotail response to prolonged southward IMF B_z intervals: Loading, unloading, and continuous magnetospheric dissipation, *J. Geophys. Res.*, *110*, A03216, doi:10.1029/2004JA010561.

Turner, N. E., W. D. Cramer, S. K. Earles, and B. A. Emery (2009), Geoefficiency and energy partitioning in CIR-driven and CME-driven storms, *J. Atmos. Sol. Terr. Phys.*, *71*, 1023–1031, doi:10.1016/j.jastp.2009.02.005.

Vassiliadis, D., A. J. Klimas, S. G. Kanekal, D. N. Baker, and R. S. Weigel (2002), Long-term-average, solar cycle, and seasonal response of magnetospheric energetic electrons to the solar wind speed, *J. Geophys. Res.*, *107*(A11), 1383, doi:10.1029/2001JA000506.

Webb, D. F., and R. A. Howard (1994), The solar cycle variation of coronal mass ejections and the solar wind mass flux, *J. Geophys. Res.*, *99*(A3), 4201–4220, doi:10.1029/93JA02742.

V. Angelopoulos, T.-S. Hsu, and R. L. McPherron, Institute of Geophysics and Planetary Physics, University of California, Los Angeles, CA 90095, USA.

J. Kissinger, Department of Earth and Space Sciences, University of California, Los Angeles, CA 90095, USA. (jkissinger@ucla.edu)